IEEE Access
Multidisciplinary | Rapid Review | Open Access Journal

Received August 8, 2020, accepted August 31, 2020, date of publication September 4, 2020, date of current version September 17, 2020.

Digital Object Identifier 10.1109/ACCESS.2020.3021694

Robust Variable Structure Anti-Slip Control Method of a Distributed Drive Electric Vehicle

BO LENG[1,2], LU XIONG[2], ZHUOPING YU[2], KAI SUN[2], AND MING LIU[2]
[1]Postdoctoral Station of Mechanical Engineering, Tongji University, Shanghai 201804, China
[2]School of Automotive Studies, Tongji University, Shanghai 201804, China

Corresponding author: Lu Xiong (xiong_lu@tongji.edu.cn)

This work was supported by the National Key Research and Development Program of China under Grant 2018YFB0104805.

ABSTRACT Slip rate control is important in improving vehicle stability and driving efficiency. In this paper, a robust slip rate control system is designed for distributed drive electric vehicles that consists of two slip rate estimators for multi-driving conditions, a vehicle speed estimator, and an anti-windup robust variable structure slip rate tracking controller. Because there is no driven wheel in a four-in-wheel-motor distributed drive electric vehicle, the estimators for small and large slip rates are designed based on dynamic and kinematic methods, respectively, which can switch according to the slip conditions. The convergence of the estimation error is discussed with the Lyapunov stability law and is less than 2% under the condition of acceleration on a low-friction road. The slip rate tracking controller is designed based on the sliding mode control law and the proportional-integral (PI) control method to handle model nonlinearity, modelling and estimation errors, and disturbances and to control the input chattering and saturation. The asymptotic stability of the tracking error is proven by Lyapunov theory. A joint control variable composed of the wheel angular acceleration and slip rate is designed to improve the robustness of the controller against the slip rate estimation error. Simulations and experiments under various conditions are performed to verify the proposed anti-slip control method. The results show that compared with a distributed drive vehicle without a slip rate controller, the controlled vehicle can prevent serious wheel skid on low-adhesion roads and improve the driving performance.

INDEX TERMS Distributed drive electric vehicle, Lyapunov stability, sliding mode control, slip rate control, slip rate estimation, vehicle speed estimation.

I. INTRODUCTION

Energy conservation and environmental protection have led to the rapid development of electric vehicles in recent years. The distributed drive electric vehicle (DDEV) with in-wheel motors has a short drive chain, high transmission efficiency, and compact structure, with an easy to realize modular design of the chassis; the DDEV is one of the most important development directions of electric vehicles [1]. In-wheel motors are fast and accurate actuators and sensors that can accurately and quickly provide speed and torque information. Through the coordinated distribution of wheel torque, a distributed drive electric vehicle equipped with four in-wheel motors can flexibly achieve various dynamic control functions.

The associate editor coordinating the review of this manuscript and approving it for publication was Chao Yang.

The anti-slip regulator (ASR), which is used to control the wheel slip rate, is one of the most significant vehicle active safety systems to prevent the vehicle from over slipping under high-acceleration and low-adhesion road conditions, leading to an improvement of vehicle safety. Traditional vehicles use an internal-combustion engine and a hydraulic braking system as actuators to realize traction control. Because of the slow response and poor control accuracy of actuators, the threshold value method has been widely applied [2]. However, this method makes the wheel slip rate chatter in a certain range, which negatively affects the stability and comfort of the vehicle.

The basic principle of anti-slip control for a DDEV is controlling the wheels in real time to track the optimal slip rate under the current tire-road attachment conditions. However, this goal is not easy to achieve due to the tire force nonlinearities and model uncertainties associated with tire and road adhesion conditions, as well as disturbances, such

as measurement noise. Compared with traditional vehicles that use internal combustion engines and hydraulic systems with slow response speeds and large dynamic performance differences to implement the ASR, DDEVs can implement the ASR based on in-wheel motors, which reduces the difficulty of control caused by actuator dynamics, which involve three main aspects: 1) Estimation of the tire-road peak friction coefficient, which determines the maximum driving force provided by the road to the tires. The reference slip rate varies with the tire-road peak friction coefficient; 2) the real-time slip rate. Since the four wheels of the DDEV are driving wheels, the vehicle speed cannot be obtained from any driven wheels. Therefore, accurate estimation of the vehicle longitudinal speed is difficult to perform in the real-time slip rate calculation; and 3) the control algorithm. According to the real-time slip rate, an appropriate motor torque should be calculated by the control algorithm to track the reference value [3].

Many scholars have successfully conducted extensive research on methods to estimate the tire-road peak friction coefficient. The estimation methods are mainly divided into three types: 1) Measuring the local stress and strain of the vehicle tire surface and using empirical formulas to analyze the instantaneous road adhesion coefficient and its corresponding changes [4]; 2) analyzing the noise between the tire and the ground to predict the tire-road friction [5], [6]; and 3) using the dynamic equation to estimate the tire-road peak friction coefficient based on the mechanical characteristics of the tire [7], [8].

Without expensive sensors, such as a high-accuracy GPS, camera and laser radar, speed estimation methods can be mainly divided into kinematic methods and dynamic methods. Both types of methods have merits and drawbacks. As a typical kinematics estimation method, the minimum-wheel-speed method uses the minimum value of four wheels as the reference speed [9], which is susceptible to the effect of the sensor precision and wheel slip condition, and the estimation accuracy greatly deteriorates on low-adhesion roads. If all the wheels are over-slipping, the method is completely ineffective. In [10], a gain matrix that adjusts the Kalman filter was proposed to estimate vehicle speed, which can detect the wheel slip rate and tune the gain matrix of the Kalman filter online. However, as the gain matrix was built based on a typical Kalman filter, its estimation performance was affected by noise from the sensors and differential operations, which greatly differed from white noise. Dynamic methods estimate the key vehicle states based on sensor information and include established dynamic models such as vehicle models and tire models. To improve the adaptability of the nonlinear system under the conditions of large slip rates or large side slip angles of tires, the adaptive extended Kalman filter (AEKF) and unscented Kalman filter (UKF) were adopted in [11], [12] for vehicle velocity estimation. Tannoury *et al.* [13] designed a variable structure observer to estimate the wheel rolling radius and rotational speed based on the nonlinear relationship between the slip rate and friction coefficient. Imsland *et al.* [14] designed a nonlinear speed observer based on the acceleration, yaw rate and wheel speeds. Because of the nonlinearity and strong coupling of the vehicle system, changes in vehicle parameters will strongly affect the accuracy of the vehicle model. Speed estimation methods, which fuse different sub-estimators or observers, were used in [15] and [16] and enhanced the robustness against sensor bias and modelling errors.

In the design of the driving torque control algorithm, ensuring the robustness against model uncertainties is an important requirement that is not easy to accomplish. A logic threshold control method based on the angular acceleration of the driving wheels and its gain coefficient was presented in [17] and has been widely used in anti-lock braking systems. However, many calibration tests are required to determine the threshold value of different working conditions. The PID control method is easy for on-board application and very attractive from an implementation viewpoint, as it has shown a significant traction performance improvement on low-adhesion roads [18], [19], but the calibration of the control parameters and stability of the control system can only be analyzed in a few cases of concern. Model predictive control has received extensive attentions in recent years. Tavernini *et al.* [20] designed an ASR for electric vehicles with in-wheel motors based on explicit nonlinear model predictive control of the wheel slip velocity and obtained better traction performance than a well-tuned PI controller. Based on the fuzzy logic control, an ASR was designed to maintain wheel slip in the optimal range using the wheel angular acceleration and slip rate [21]. However, the effect of fuzzy logic control depends on the accuracy of the empirical function, which indicates that it is difficult to establish control rules. Sliding mode control is robust to model uncertainties and nonlinearities [22], so it is suitable for slip rate control, such as in the anti-lock braking system [23], hybrid braking system [24] and traction control system [25]. Sliding mode control divides the control moment into an equivalent moment and a switching moment. The design of the switching moment includes an uncertain upper bound and an approaching term, which cover the model uncertainty and external disturbance, to ensure that the system state can converge to the sliding mode surface. To reduce chattering near the sliding mode surface, the high-order sliding mode variable structure method is generally adopted [26], and the symbolic function is replaced by the saturation function or continuous functions [27]. However, there is a lack of a complete theoretical proof for the stability of the sliding mode control system with a variable structure. Although sliding mode control is robust to uncertainties, the slip rate as a control variable has an estimation error, so a method to ensure the effect of slip rate control requires further study.

The main contributions of this article are: 1) Slip rate and vehicle speed estimators based on dynamic and kinematic methods are built and integrated according to the characteristics of the different estimation methods. The kinematic estimation method for large-slip-rate conditions is

designed to avoid the deterioration of the estimation accuracy caused by tire modelling errors. Because wheels normally always run in a small-slip-rate range, the dynamic estimation method is designed to avoid sensor error accumulation. A reasonable switching mechanism for the two estimation methods is designed to improve the smoothness and accuracy of the speed estimation. 2) A sliding mode variable structure controller against integral saturation is designed to realize slip rate tracking control, in which the sliding mode algorithm can quickly converge the slip rate to the boundary layer when the slip rate is too large and the anti-windup PI algorithm in the boundary layer can stabilize the tracking error. Inspired by [28], the global asymptotic stability of the variable structure controller for driving anti-slip is proven with Lyapunov stability theory. In addition, a joint control variable that combines wheel angular acceleration and the slip rate is designed, which can effectively suppress the deterioration of the slip rate control effect caused by the speed estimation error. 3) The designed controller is verified in various simulations and field tests.

The remainder of the article is organized as follows: In Section II, the tire slip rate and vehicle speed estimation methods are introduced. The design and proven progress of the slip rate controller are presented in Section III. The tire-road peak friction coefficient is estimated by the authors' team in [29] and assumed to be known in this paper. In Section IV, simulation and field tests results are presented. Conclusions are drawn in Section V.

II. TIRE SLIP RATE AND VEHICLE SPEED ESTIMATION

In this section, based on the situation of tire slip, two slip rate estimation methods under different working conditions are designed to reduce estimation errors. The characteristics of the error convergence under the two estimators are analyzed. Finally, the vehicle longitudinal speed is estimated based on the slip rate estimation results of the four wheels.

A. DYNAMIC SLIP RATE ESTIMATION METHOD

In the case of a small slip rate, the tire model can be approximately considered to be a linear model, and the longitudinal slip stiffness fitting error based on the tire test is small. The four-wheel drive electric vehicle must obtain speed information through the estimator throughout the driving process, and the wheels do not quickly slip under most driving conditions. Therefore, a dynamic estimation method with a better estimation accuracy and without cumulative errors is appropriate.

Under the driving conditions, the slip rate is defined as:

$$\lambda = \frac{\omega r_w - v_w}{\omega r_w} \tag{1}$$

where, ω is the wheel speed, v_w is the velocity at the center of the wheel, and r_w is the rolling radius.

As shown in (2), the longitudinal acceleration at the center of the wheel is obtained by considering vehicle steering and neglecting tire sideslip.

$$\begin{aligned} \dot{v}_{w,fl} &= \frac{\dot{v}_x - 0.5 b_f \dot{\gamma}}{\cos\delta_f}, \quad \dot{v}_{w,fr} = \frac{\dot{v}_x + 0.5 b_f \dot{\gamma}}{\cos\delta_f} \\ \dot{v}_{w,rl} &= \dot{v}_x - 0.5 b_r \dot{\gamma}, \quad \dot{v}_{w,rr} = \dot{v}_x + 0.5 b_r \dot{\gamma} \end{aligned} \tag{2}$$

where, v_x is the vehicle longitudinal speed; γ is the yaw rate; b_f and b_r are the front wheel track and rear wheel track, respectively; δ_f is the steering angle; $i = fl, fr, rl, rr$ refers to the front left, front right, rear left and rear right wheels (the same as below), respectively.

To simplify the expression, assuming the vehicle travels in a straight line. Then, (2) can be expressed as:

$$\dot{v}_{w,i} = \dot{v}_x \tag{3}$$

Based on the single-wheel model shown in Figure 1, the dynamic equation of wheel rotation is obtained:

$$J_w \dot{\omega} = T - F_x r_w = T - r_w F_z \mu(\lambda) \tag{4}$$

where, J_w is the equivalent moment of inertia at the wheel, T is the wheel torque, F_x is the tire longitudinal force, F_z is the tire vertical load, and $\mu(\lambda)$ is the product of the normalized longitudinal slip stiffness and slip rate under the current road surface and the slip rate obtained based on the tire model.

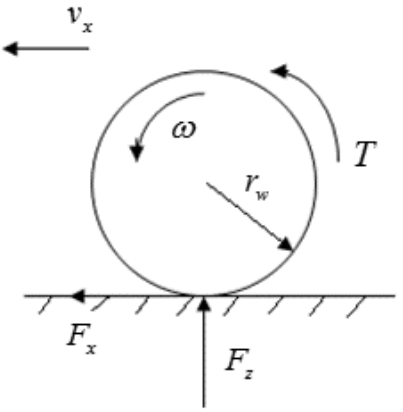

FIGURE 1. Single-wheel model.

According to the derivatives of (1), (3) and (4), the dynamic equation for the slip rate is:

$$\begin{aligned} \dot{\lambda} &= (1 - \frac{v_x}{\omega r_w})' = (1-\lambda)\frac{\dot{\omega}}{\omega} - \frac{\dot{v}_x}{\omega r_w} \\ &= (1-\lambda)\frac{T - r_w F_z \mu(\lambda)}{J_w \omega} - \frac{\dot{v}_x}{\omega r_w} \end{aligned} \tag{5}$$

The dynamic observer is designed as follows:

$$\begin{aligned} \dot{\hat{\lambda}} &= (1-\hat{\lambda})\frac{\dot{\hat{\omega}}}{\omega} - \frac{\dot{\hat{v}}_x}{\omega r_w} \\ &= (1-\hat{\lambda})\frac{T - r_w \hat{F}_z \hat{\mu}(\hat{\lambda})}{J_w \omega} - \frac{\dot{\hat{v}}_x}{\omega r_w} \end{aligned} \tag{6}$$

where, $\hat{F}_z, \hat{\mu}, \hat{\lambda}$ represent the estimated values of the corresponding variables; $\hat{\dot{v}}_x$ is the measured value of the acceleration sensor. The estimated vertical load of each wheel is:

$$\begin{aligned} F_{z,fl} &= mg\frac{l_r}{2l} - m\frac{h_g}{2l}a_x - m\frac{h_g l_r}{b_f l}a_y \\ F_{z,fr} &= mg\frac{l_r}{2l} - m\frac{h_g}{2l}a_x + m\frac{h_g l_r}{b_f l}a_y \\ F_{z,rl} &= mg\frac{l_f}{2l} + m\frac{h_g}{2l}a_x - m\frac{h_g l_f}{b_f l}a_y \\ F_{z,rr} &= mg\frac{l_f}{2l} + m\frac{h_g}{2l}a_x + m\frac{h_g l_f}{b_r l}a_y \end{aligned} \tag{7}$$

where, $g = 9.8m/s^2$ is the gravitational acceleration; m is the vehicle mass; h_g is the height of the center of gravity (CoG); l_f and l_r are the distances from the front axle and rear axle to the CoG, respectively; $l = l_f + l_r$ is the wheelbase; a_x is the longitudinal acceleration; and a_y is the lateral acceleration.

Define $\tilde{x} = \hat{x} - x$ to be the error between the true value of x and its estimated or measured value $\hat{x}$.

The derivative of the slip rate estimation error $\dot{\tilde{\lambda}} = \dot{\hat{\lambda}} - \dot{\lambda}$ can be obtained from (5) and (6):

$$\begin{aligned} \dot{\tilde{\lambda}} &= -\frac{r_w}{J_w\omega}[\hat{F}_z\hat{\mu}(\hat{\lambda}) - F_z\mu(\lambda)] - \frac{T}{J_w\omega}\tilde{\lambda} - \frac{\tilde{a}_x}{\omega r_w} \\ &\quad + \frac{r_w}{J_w\omega}\hat{F}_z\hat{\mu}(\hat{\lambda})\hat{\lambda} - \frac{r_w}{J_w\omega}F_z\mu(\lambda)\lambda \\ &= -[(1-\lambda) - \tilde{\lambda}]\frac{r_w}{J_w\omega}\hat{F}_z\hat{\mu}(\hat{\lambda}) + (1-\lambda)\frac{r_w}{J_w\omega}F_z\mu(\lambda) \\ &\quad - \frac{T}{J_w\omega}\tilde{\lambda} - \frac{\tilde{a}_x}{\omega r_w} \\ &= \frac{(1-\lambda)r_w}{J_w\omega}[F_z\mu(\lambda) - \hat{F}_z\hat{\mu}(\hat{\lambda})] + \frac{r_w\hat{F}_z\hat{\mu}(\hat{\lambda}) - T}{J_w\omega}\tilde{\lambda} - \frac{\tilde{a}_x}{\omega r_w} \\ &= \frac{(1-\lambda)r_w}{J_w\omega}\{[F_z\mu(\lambda) - F_z\mu(\hat{\lambda})] + [F_z\mu(\hat{\lambda}) - \hat{F}_z\mu(\hat{\lambda})] \\ &\quad + [\hat{F}_z\mu(\hat{\lambda}) - \hat{F}_z\hat{\mu}(\hat{\lambda})]\} + \frac{r_w\hat{F}_z\hat{\mu}(\hat{\lambda}) - T}{J_w\omega}\tilde{\lambda} - \frac{\tilde{a}_x}{\omega r_w} \\ &= \frac{1}{J_w\omega}[-r_wF_zC_x(1-\lambda) + r_w\hat{F}_z\hat{\mu}(\hat{\lambda}) - T]\tilde{\lambda} \\ &\quad + \frac{(1-\lambda)r_w}{J_w\omega}[-\tilde{F}_z\mu(\hat{\lambda}) - \hat{F}_z\tilde{\mu}] - \frac{\tilde{a}_x}{\omega r_w} \end{aligned} \tag{8}$$

Considering the wheel dynamics described in (4), equation (8) can be rewritten as

$$\begin{aligned} \dot{\tilde{\lambda}} &= -\frac{r_wF_zC_x(1-\lambda) + J_w\dot{\hat{\omega}}}{J_w\omega}\tilde{\lambda} \\ &\quad + \frac{(1-\lambda)r_w}{J_w\omega}[-\tilde{F}_z\mu(\hat{\lambda}) - \hat{F}_z\tilde{\mu} - \frac{\tilde{a}_xJ_w}{(1-\lambda)r_w^2}] \end{aligned} \tag{8'}$$

According to the coefficient of each term in (8)′, the slip rate estimation error is convergent and bounded under the acceleration conditions. In particular, when the slip rate is overestimated ($\tilde{\lambda} = \hat{\lambda} - \lambda > 0$), the Lyapunov function is constructed as:

$$V = \frac{1}{2}\tilde{\lambda}^2 \tag{9}$$

Then

$$\begin{aligned} \dot{V} = \tilde{\lambda}\dot{\tilde{\lambda}} &= -\frac{r_wF_zC_x(1-\lambda) + J_w\dot{\hat{\omega}}}{J_w\omega}\tilde{\lambda}^2 \\ &\quad + \frac{(1-\lambda)r_w}{J_w\omega}[-\tilde{F}_z\mu(\hat{\lambda}) - \hat{F}_z\tilde{\mu} - \frac{\tilde{a}_xJ_w}{(1-\lambda)r_w^2}]\tilde{\lambda} < 0 \end{aligned} \tag{10}$$

Thus, the slip rate estimation error is asymptotically stable to the extent that the tire model can be considered linear. Therefore, when the slip rate is in a reasonably small range, it can be estimated based on the dynamic model. However, when the slip rate is large, its value estimated by the dynamic method is not reliable, so the kinematic method is proposed.

B. KINEMATIC SLIP RATE ESTIMATION METHOD

According to the previous analysis, at large slip rates, the tire modelling error may be large, so a slip rate estimator is constructed based on the kinematic equation. In addition, to avoid cumulative errors of the sensor signal, the working duration of the kinematic estimator should not be too long, which can be ensured by using it in combination with the slip rate controller and switching strategy.

The kinematic estimator is designed according to the slip rate differential equation in (5):

$$\dot{\hat{\lambda}} = (1-\hat{\lambda})\frac{\dot{\hat{\omega}}}{\omega} - \frac{\dot{\hat{v}}_x}{\omega r_w} \tag{11}$$

From (5) and (11), we obtain:

$$\begin{aligned} \dot{\tilde{\lambda}} = \dot{\hat{\lambda}} - \dot{\lambda} &= (1-\hat{\lambda})\frac{\dot{\hat{\omega}}}{\omega} - (1-\lambda)\frac{\dot{\omega}}{\omega} - \frac{\dot{\hat{v}}_x}{\omega r_w} + \frac{\dot{v}_x}{\omega r_w} \\ &= -\frac{\dot{\hat{\omega}}}{\omega}\tilde{\lambda} + (1-\lambda)\frac{\tilde{\dot{\omega}}}{\omega} - \frac{\tilde{a}_x}{\omega r_w} \end{aligned} \tag{12}$$

The boundary of the solution of (12), i.e., $\tilde{\lambda}$, can be expressed as

$$\begin{aligned} \left\|\tilde{\lambda}\right\| \le \left\|\tilde{\lambda}\left(t_0\right)\right\| \cdot \exp\left[-\frac{\dot{\hat{\omega}}}{\omega}\cdot(t-t_0)\right] \\ + \sup_{t_0\le\tau\le t}\frac{1}{\hat{\omega}}\cdot\left[(1-\lambda)\left\|\tilde{\dot{\omega}}\right\| + \frac{\|\tilde{a}_x\|}{r_w}\right] \end{aligned} \tag{13}$$

Analysis (13): 1) When the wheel seriously slips, $\hat{\omega}$ becomes large and results in a large $\dot{\hat{\omega}}/\dot{\omega}$. Thus, the initial error of the exponential term converges. However, the intervention of the ASR will reduce the very large $\dot{\hat{\omega}}$ in a short time, which causes a large steady-state error in the estimation of the slip rate, especially when the initial error $\left\|\tilde{\lambda}\left(t_0\right)\right\|$ is large, i.e., the first exponential term does not have sufficient time to converge to zero. Thus, when we switch from the dynamic estimation method to the kinematic estimation method, it is necessary to ensure timely switching to obtain a small initial estimation error of the slip rate.

2) The steady-state error of (13) is mainly caused by:

2.1) The calculation error of the wheel angular acceleration. This term can be considered to have a mean value of zero, so it will not cause a cumulative error to the steady-state

value, but it will make the estimated value jitter near the true value.

2.2) Acceleration zero drift. Because the slip time is short, $\hat{\dot{\omega}}$ does not maintain a large value. When $\hat{\dot{\omega}}$ decreases, $\|\tilde{a}_x\| \Big/ \left(\hat{\dot{\omega}}_i r\right)$ gradually increases and causes a large steady-state error. Therefore, to avoid the continuous accumulation of errors, the kinematic estimator should be withdrawn in time and switched to the dynamic estimator.

C. SLIP RATE ESTIMATOR SWITCHING STRATEGY

The switching strategy of the dynamic estimator and kinematic estimator is designed as shown in Figure 2, in which the wheel angular acceleration is used as the main criterion, and is associated with the wheel speed threshold.

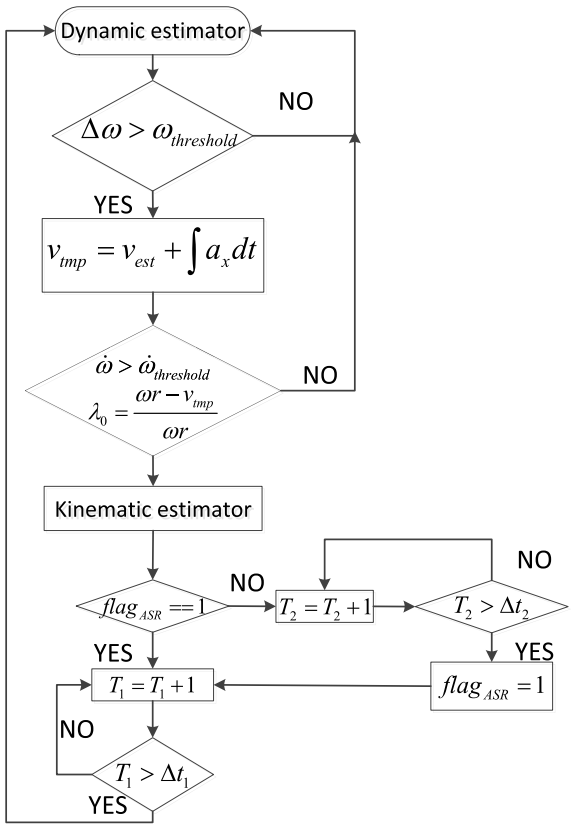

FIGURE 2. Logic diagram of the slip rate estimator switching strategy.

The switching process is as follows:

1) When it is determined from the wheel speed signal that the wheel speed is rapidly increasing, i.e., the difference in the wheel speed at time k [$\omega(k)$] and time *(k-1)* [$\omega(k-1)$] is larger than a threshold $\omega_{threshold}$, it enters the ready state for switching. At this moment, the estimated value of the vehicle speed v_{est} is recorded, and a temporary vehicle speed v_{tem} based on the integral of longitudinal acceleration is obtained:

$$\omega(k) - \omega(k-1) > \omega_{threshold}$$
$$v_{tmp}(k+m) = v_{est}(k) + \sum_{i=0}^{m} a_x(k+i)\Delta t$$

2) The noise in wheel speed measurement will cause a misjudgement if the wheel speed is the only criterion. Therefore, it is determined that the wheel begins to skid after both the wheel speed variation and wheel angular acceleration have reached the thresholds. At this moment, the temporary vehicle speed and current wheel speed are used to calculate the current slip rate and replace the estimated value:

$$\dot{\omega}(k) > \dot{\omega}_{threshold}$$
$$v\_acc(k+m) = v_{tmp}(k) + \sum_{i=0}^{m} a_x(k+i)\Delta t$$
$$\lambda_{est}(k) = \frac{\omega(k) r_w - v\_acc(k)}{\omega(k) r_w}$$

3) After the kinematics estimator is used, we must confirm whether the slip rate controller is involved at this time. If the slip rate controller intervenes ($flag_{ASR} = 1$), then the kinematic estimator exits, and the dynamic estimation method works after the slip rate controller has worked for a time period Δt_1. If the slip rate controller does not intervene ($flag_{ASR} = 0$), then prevent deterioration of the estimation result caused by long-term operation under large-slip-rate conditions, the slip rate controller is actively activated after Δt_2. Then, the kinematic estimator exits, and the dynamic estimator works instead after the slip rate controller has worked for a time period Δt_1.

D. VEHICLE SPEED ESTIMATION

Because the slip rate estimation result may jitter during the convergence progress, the vehicle speed directly calculated by the estimated slip rate will abruptly change. A wheel center speed estimator is designed in (14). The vehicle longitudinal speed is obtained by fusing the center speeds of the four wheels.

$$\dot{\hat{v}}_{x,i} = \xi \cdot sat\left\{\frac{a_x}{\xi} - \frac{L}{\xi}\left[\frac{\hat{v}_{x,i}}{(1-\hat{\lambda}_i) r_w} - \omega\right]\right\}, \quad (i = fl, fr, rl, rr) \tag{14}$$

where, $\hat{v}_{x,i}$ and λ_i are the estimated center speed and the slip rate of the corresponding wheel, respectively. The physical meaning of the saturation function is that the longitudinal acceleration is less than ξ, and $L > 0$ is the estimator parameter. The estimation error dynamics are

$$\begin{aligned}\dot{\tilde{v}}_{x,i} &= \dot{\hat{v}}_{x,i} - \dot{v}_{x,i} \\ &= -\frac{L}{(1-\lambda_i) r_w}\tilde{v}_{x,i} - \frac{L\hat{v}_{x,i}\tilde{\lambda}_i}{(1-\lambda_i)(1-\hat{\lambda}_i) r_w} + \tilde{a}_x\end{aligned} \tag{15}$$

By analysing the coefficients of (15), it can be seen that the vehicle speed estimation error is converged and bounded as shown in (16)

$$\begin{aligned}\left\|\tilde{v}_{x,i}\right\| \le \|\tilde{v}_{x0}\|\, e^{-\frac{L}{r_w(1-\lambda_i)}(t-t_0)} \\ + \sup_{t_0 \le \tau \le t}\left[\frac{\hat{v}_i}{1-\hat{\lambda}_i} \cdot \left\|\tilde{\lambda}_i\right\| + \frac{r_w(1-\lambda_i)}{L} \cdot \|\tilde{a}_x\|\right]\end{aligned} \tag{16}$$

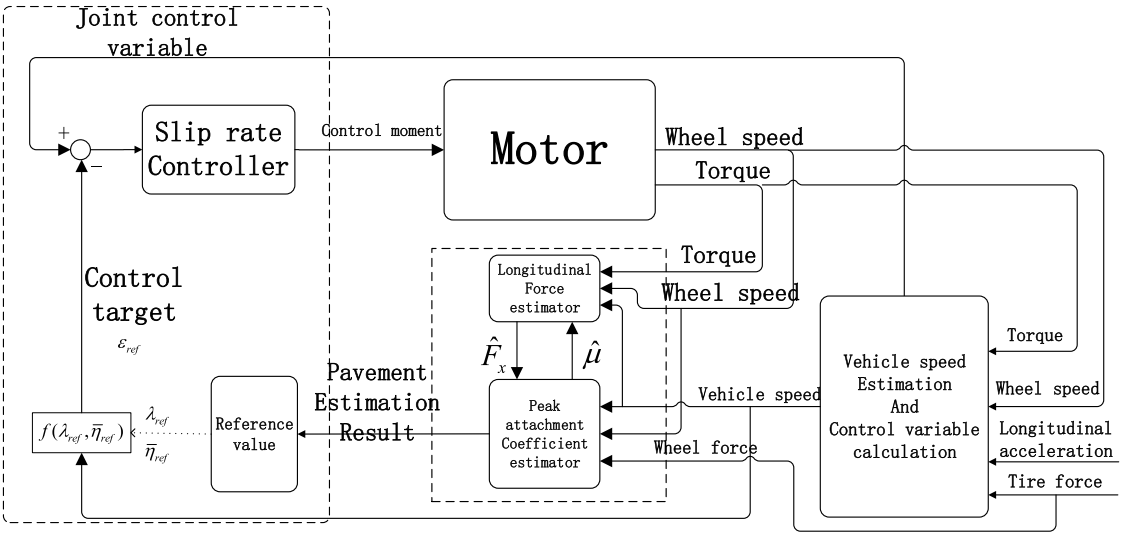

FIGURE 3. Block diagram of the slip rate controller.

As shown in (17), the estimated wheel center speeds $v_{x,i}$ are converted into the longitudinal speed v_x at the CoG.

$$
\begin{aligned}
v_x &= \begin{cases} \frac{1}{4}\left(v_{x,fl}+v_{x,fr}+v_{x,rl}+v_{x,rr}\right), FLAG=4 \\ \frac{1}{H}\left(\eta_{fl}v_{x,fl}+\eta_{fr}v_{x,fr}+\eta_{rl}v_{x,rl}+\eta_{rr}v_{x,rr}\right), \\ \quad FLAG\neq 4 \end{cases} \\
\eta_i &= \mu_i/\lambda_i\cdot(2-flag_i), i=fl,fr,rl,rr \\
H &= \eta_{fl}+\eta_{fr}+\eta_{rl}+\eta_{rr} \\
flag_i &= \begin{cases} 0, & \text{Dynamic slip rate estimator works} \\ 1, & \text{Kinematic slip rate estimator works} \end{cases} \\
FLAG &= flag_{fl}+flag_{fr}+flag_{rl}+flag_{rr}
\end{aligned} \tag{17}
$$

where, μ is the tire-road peak friction coefficient.

The principles of the calculation of v_x are:

1) When all four wheels adopt the kinematic estimation method, the average value of the four estimated vehicle speeds is used as the estimated longitudinal vehicle speed.

2) Since the dynamic estimator works under the small-slip-rate condition with an accurate tire model, it outputs precise results and has a greater weight factor than the kinematic estimator. Furthermore, for multiple wheels using dynamic slip rate estimators, a larger μ/λ corresponds to a more strictly linear tire characteristic curve and a greater weighting coefficient in the vehicle speed fusion process.

III. SLIP RATE CONTROLLER

Based on the estimation results presented in Section II, a robust adaptive anti-integral saturation variable structure controller of the slip rate is designed.

A. SLIDING MODE VARIABLE STRUCTURE CONTROL LAW

According to the quarter vehicle model shown in Figure 4:

$$
\begin{aligned}
J_w\dot{\omega} &= T_d - r_wF_x \\
m_w\dot{v}_x &= F_x - f
\end{aligned} \tag{18}
$$

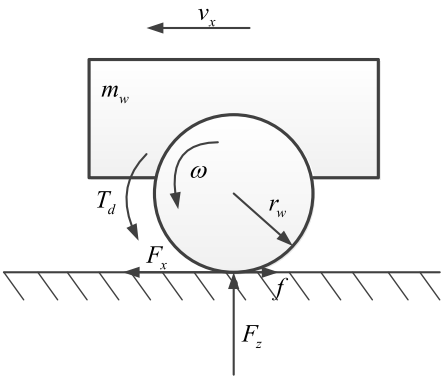

FIGURE 4. Quarter vehicle model.

where, $T_d > 0$ is the desired driving torque from an upper control layer, m_w is the equivalent mass of a quarter vehicle and f is the rolling resistance.

In (5), the design control input is $u \in [0, 1]$; then, the wheel driving torque is $T = uT_d$, and

$$
\dot{\lambda} = -\frac{r_w}{vJ_w}(1-\lambda)^2\left[\left(\frac{J_w}{m_wr_w^2}\cdot\frac{1}{1-\lambda}+1\right)r_wF_z\mu(\lambda)-uT_d\right] \tag{19}
$$

Define

$$
\begin{aligned}
\tilde{\kappa} &= \frac{r_w}{vJ_w}(1-\lambda)\geq 0 \\
\psi(\lambda) &= \left(\frac{J_w}{m_wr_w^2}\cdot\frac{1}{1-\lambda}+1\right)r_wF_z\mu(\lambda) \\
\tilde{\psi}(\lambda) &= \left(\frac{J_w}{m_wr_w^2}+1-\lambda\right)r_wF_z\mu(\lambda)
\end{aligned} \tag{20}
$$

Obtain:

$$
\dot{\lambda} = -\tilde{\kappa}\left[\tilde{\psi}(\lambda)-uT_d\,(1-\lambda)\right] \tag{21}
$$

Design control law:

$$\begin{aligned} u &= \frac{1}{T_d}\left[\hat{\psi}(\lambda) - T_d B sat(\frac{s}{\theta})\right] \\ s &= e + k_0\sigma \\ \dot{\sigma} &= -k_0\sigma + \theta sat(\frac{s}{\theta}), |\sigma(0)| \le \frac{\theta}{k_0} \\ e &= \lambda - \lambda_{ref} \end{aligned} \tag{22}$$

where, controller parameters k_0 and θ are positive real numbers decided by calibration, k_0 is the scale factor and θ is the boundary layer thickness. $\hat{\psi}(\lambda)$ is the estimated value of $\tilde{\psi}(\lambda)$ and satisfies

$$\frac{\left|\hat{\psi}(\lambda) - \tilde{\psi}(\lambda)\right|}{T_d} \le \rho(\lambda), \quad \forall\lambda \in D = [0, 1] \tag{23}$$

and

$$B = \rho(\lambda) + B_0, B_0 > 0 \tag{24}$$

B. STABILITY PROOF

Lemma 1 and **Lemma 2** are proposed.

Lemma 1: Define set $D_\sigma = \{|\sigma| \le \theta/k_0\}$, where $\dot{\sigma} = -k_0\sigma + \theta sat(s/\theta)$ and $\sigma(0) \in D_\sigma$ is a positive invariant set, which implies that $\sigma(t) \in D_\sigma, \forall t \ge 0$.

Proof:

Design the Lyapunov function

$$V = \frac{1}{2}\sigma^2 \tag{25}$$

then

$$\dot{V} = \sigma\dot{\sigma} = \sigma \cdot [-k_0\sigma + \theta sat(s/\theta)] \tag{26}$$

At the boundary of D_σ, $\{-\theta/k_0, \theta/k_0,\}$, there are

$$\begin{aligned} \dot{V}(-\frac{\theta}{k_0}) &= -\frac{\theta^2}{k_0} - \frac{\theta^2}{k_0} \cdot sat\left(\frac{s}{\theta}\right) \le -\frac{\theta^2}{k_0} - \frac{\theta^2}{k_0} \cdot (-1) \le 0 \\ \dot{V}(\frac{\theta}{k_0}) &= -\frac{\theta^2}{k_0} + \frac{\theta^2}{k_0} \cdot sat\left(\frac{s}{\theta}\right) \le -\frac{\theta^2}{k_0} - \frac{\theta^2}{k_0} \cdot 1 = 0 \end{aligned} \tag{27}$$

Thus, D_σ is a positive invariant set. ■

Lemma 2: Define set $\Pi_\theta = \{(e, \sigma) \in D_e \times D_\sigma : |s(e, \sigma)| \le \theta\}$, there is $sat(s/e) = sgn(e)$ when $(e, \sigma) \notin \Pi_\theta$.

Proof:

When $(e, \sigma) \notin \Pi_\theta$, i.e., $|s| > \theta$, there is

$$sat(s/e) = sgn(s) = sgn(e + k_0\sigma)$$

According to Lemma 1, $\sigma(t) \in D_\sigma, \forall t \ge 0$. Define set

$$\Sigma = \{(e, \sigma) : |e + k_0\sigma| > \theta, k_0|\sigma| \le \theta\} \tag{28}$$

Divide Σ into

$$\begin{aligned} \Sigma_+ &= = \{(e, \sigma) : e + k_0\sigma > \theta, k_0|\sigma| \le \theta\} \\ \Sigma_- &= \{(e, \sigma) : e + k_0\sigma < -\theta, k_0|\sigma| \le \theta\} \end{aligned} \tag{29}$$

$\forall (e, \sigma) \in \Sigma_+, \exists e + k_0\sigma > \theta \Rightarrow e > \theta - k_0\sigma \ge \theta - \theta = 0.$

$sgn(e + k_0\sigma) = sgn(e) = 1.$

$\forall (e, \sigma) \in \Sigma_-, \exists e + k_0\sigma < -\theta \Rightarrow e < -\theta - k_0\sigma \le -\theta - (-\theta) = 0.$

$sgn(e + k_0\sigma) = sgn(e) = -1.$

Based on the previous analysis, $sgn(e + k_0\sigma) = sgn(e)$ when $(e, \sigma) \in \Sigma_+ \cup \Sigma_-$, which means $sat(s/e) = sgn(e)$ when $(e, \sigma) \notin \Pi_\theta$. ■

Theorem: When the control law designed in (22) satisfies (23),

1) $\forall (e(0), \sigma(0)) \in D_e \times D_\sigma$ can converge to the set Π_θ within a finite amount of time;

2) In the set Π_θ, the equilibrium point $(\bar{e}, \bar{\sigma})$ described in (30) is asymptotically stable.

$$\left(\bar{e} = 0, \bar{\sigma} = -\frac{\theta}{k_0\left[\rho(\lambda_{ref}) + B_0\right]} \cdot \Delta\left(\lambda_{ref}\right)\right) \tag{30}$$

where, $\Delta(\lambda) = \frac{\left|\hat{\psi}(\lambda) - \tilde{\psi}(\lambda)\right|}{T_d}$ and $\frac{\Delta(\lambda)}{\rho(\lambda) + B_0}$ satisfy the Lipschitz condition.

Proof:

1) According to **Lemma 1**, D_σ is a positive invariant set. Design the Lyapunov function

$$V = \frac{1}{2}e^2 \tag{31}$$

then

$$\dot{V} = e\dot{e} = e\dot{\lambda} = -e\tilde{\kappa}\left\{\tilde{\psi}(\lambda) - (1 - \lambda)\left[\hat{\psi}(\lambda) - T_d B sat(\frac{s}{\theta})\right]\right\} \tag{32}$$

When $(e, \sigma) \notin \Pi_\theta$, according to **Lemma 2**, there is:

$$\begin{aligned} \dot{V} &\le -e\tilde{\kappa}\left\{(1 - \lambda)\,\tilde{\psi}(\lambda) - (1 - \lambda)\left[\hat{\psi}(\lambda) - T_d B sgn(e)\right]\right\} \\ &= -e\tilde{\kappa}\,(1 - \lambda)\,T_d\left[\frac{\tilde{\psi}(\lambda) - \hat{\psi}(\lambda)}{T_d} + B sgn(e)\right] \\ &\le -\tilde{\kappa}\,(1 - \lambda)\,T_d B_0\,|e| \le 0 \end{aligned} \tag{33}$$

$\because \forall (e(0), \sigma(0)) \in D_e \times D_\sigma$, the set Π_θ can be reached within a finite amount of time.

2)

2-a) When $(e, \sigma) \notin \Pi_\theta$ and $e \ne 0$,

$$\begin{aligned} \dot{\sigma} &= e \\ \dot{e} = \dot{\lambda} &= -\tilde{\kappa}\left[\tilde{\psi}(\lambda) - (1 - \lambda)\,\hat{\psi}(\lambda) + T_d B(\frac{e + k_0\sigma}{\theta})\right] \end{aligned} \tag{34}$$

Define

$$\tilde{\sigma} = \sigma - \bar{\sigma}, \tilde{s} = s - \bar{s}, \bar{s} = \bar{e} + k_0\bar{\sigma} = k_0\bar{\sigma} \tag{35}$$

The Lyapunov function is

$$V = \frac{1}{2}\tilde{s}^2 + \frac{1}{2}\tilde{\sigma}^2 \tag{36}$$

then

$$\begin{aligned}\dot{V} &= \tilde{s}\dot{\tilde{s}} + \tilde{\sigma}\dot{\tilde{\sigma}} = \tilde{s}\dot{s} + \tilde{\sigma}\dot{\sigma} = \tilde{s}\left(\dot{e} + k_0 e\right) + \tilde{\sigma} e \\ &= -\tilde{s}\tilde{\kappa}\left[\tilde{\psi}(\lambda) - (1-\lambda)\,\hat{\psi}(\lambda) + T_d \cdot B(\lambda) \cdot \left(\frac{e + k_0\sigma}{\theta}\right)\right] \\ &\quad + \tilde{s}k_0 e + \tilde{\sigma} e \end{aligned} \tag{37}$$

Substitute $e = \tilde{s} - k_0\tilde{\sigma}$ in (37), get

$$\begin{aligned}\dot{V} &= -\tilde{s}\tilde{\kappa}\left[\tilde{\psi}(\lambda) - (1-\lambda)\,\hat{\psi}(\lambda) + T_d \cdot B(e+\lambda_{ref}) \cdot \left(\frac{\tilde{s}+\bar{s}}{\theta}\right)\right] \\ &\quad + k_0\tilde{s}(\tilde{s} - k_0\tilde{\sigma}) + \tilde{\sigma}(\tilde{s} - k_0\tilde{\sigma}) \\ &= -\left[\tilde{\kappa}T_d\frac{B(e+\lambda_{ref})}{\theta} - k_0\right]\tilde{s}^2 \\ &\quad - \tilde{\kappa}\tilde{s}T_d\left[\frac{\tilde{\psi}(\lambda) - (1-\lambda)\,\hat{\psi}(\lambda)}{T_d} + B(e+\lambda_{ref})\frac{\bar{s}}{\theta}\right] \\ &\quad - (k_0^2 - 1)\tilde{s}\tilde{\sigma} - k_0\tilde{\sigma}^2 \end{aligned} \tag{38}$$

In (38), define

$$\begin{aligned}\bar{s} = k_0\bar{\sigma} &= \frac{-\theta \cdot \Delta(\lambda_{ref})}{B(\lambda_{ref})} \\ \chi(\lambda) &= \tilde{\kappa}T_d B(\lambda_{ref})\end{aligned}$$

then

$$\begin{aligned}\dot{V} &= -\left[\frac{\chi(e+\lambda_{ref})}{\theta} - k_0\right]\tilde{s}^2 - \chi(e+\lambda_{ref}) \\ &\quad \times \tilde{s}\frac{\tilde{\psi}(\lambda) - (1-\lambda)\,\hat{\psi}(\lambda)}{T_d B(e+\lambda_{ref})} \\ &\quad - \chi(e+\lambda_{ref})\tilde{s}\frac{\Delta(\lambda_{ref})}{B(\lambda_{ref})} - (k_0^2-1)\tilde{s}\tilde{\sigma} - k_0\tilde{\sigma}^2 \\ &\le -\left[\frac{\chi(e+\lambda_{ref})}{\theta} - k_0\right]\tilde{s}^2 - (k_0^2-1)\tilde{s}\tilde{\sigma} - k_0\tilde{\sigma}^2 \\ &\quad + \chi(e+\lambda_{ref})\,|\tilde{s}| \\ &\quad \cdot \left|\frac{\Delta(e+\lambda_{ref})}{B(e+\lambda_{ref})} - \frac{\Delta(\lambda_{ref})}{B(\lambda_{ref})} + \frac{\lambda\hat{\psi}(\lambda)}{T_d B(e+\lambda_{ref})}\right| \end{aligned} \tag{39}$$

where,

$$\left|\frac{\Delta(e+\lambda_{ref})}{B(e+\lambda_{ref})} - \frac{\Delta(\lambda_{ref})}{B(\lambda_{ref})} + \frac{\lambda\hat{\psi}(\lambda)}{T_d B(e+\lambda_{ref})}\right| \le L\,|e| + \theta \tag{40}$$

Because θ is bounded, $N > L$ can be found and makes $L\,|e| + \theta \le N\,|e|$ when $e \ne 0$.

$$\begin{aligned}\dot{V} &\le -\left[\frac{\chi(e+\lambda_{ref})}{\theta} - k_0 - N\chi(e+\lambda_{ref})\right]\tilde{s}^2 \\ &\quad + \left[k_0^2 + 1 + N\chi(e+\lambda_{ref})\right]|\tilde{s}|\,|\tilde{\sigma}| - k_0\tilde{\sigma}^2 \\ &\Rightarrow \dot{V} \le -\begin{bmatrix}|\tilde{\sigma}| & |\tilde{s}|\end{bmatrix} P \begin{bmatrix}|\tilde{\sigma}| \\ |\tilde{s}|\end{bmatrix} \\ P &= \begin{bmatrix} k_0 & -\frac{k_0^2+1+N\chi(e+\lambda_{ref})}{2} \\ -\frac{k_0^2+1+N\chi(e+\lambda_{ref})}{2} & \chi(e+\lambda_{ref})\left(\frac{1}{\theta} - N\right) - k_0 \end{bmatrix} \end{aligned} \tag{41}$$

(42) exists and makes matrix $\boldsymbol{P}$ negative definite.

$$\begin{aligned}&k_0 > 0, \theta \in \left(0, \theta^*\right) \\ &\theta^* = \min_{e\in D_e}[N + \frac{k_0}{\chi(e+\lambda_{ref})} \\ &\quad + \frac{1}{k_0\chi(e+\lambda_{ref})}(\frac{1+k_0^2+Nk_0\chi(e+\lambda_{ref})}{2})^2]^{-1} \end{aligned} \tag{42}$$

2-b) When $e = 0$, $\tilde{s} = s - \bar{s} = e + k_0\sigma - k_0\bar{\sigma} = k_0\tilde{\sigma}$, then

$$\begin{aligned}\dot{V} &= \tilde{s}\dot{\tilde{s}} + \tilde{\sigma}\dot{\tilde{\sigma}} = k_0\tilde{\sigma}\cdot k_0\dot{\tilde{\sigma}} + \tilde{\sigma}\dot{\tilde{\sigma}} \\ &= \left(k_0^2\tilde{\sigma} + \tilde{\sigma}\right)\dot{\tilde{\sigma}} = \left(k_0^2\tilde{\sigma} + \tilde{\sigma}\right)\dot{\sigma} = 0 \end{aligned} \tag{43}$$

From 2-a) and 2-b) the second characteristic in the **Theorem** is proven.

Via the analyses of 1) and 2), the **Theorem** is proven. ■

C. JOINT CONTROL VARIABLE

There are inevitable errors in the slip rate estimation caused by model error, sensor zero drift and disturbances. Therefore, the wheel speed information directly measured by the sensor is used to introduce wheel angular acceleration into the control variable to improve the problem of the decrease of the control effect, which may be caused by the slip rate as the single control variable.

According to (5), the derivative of the slip rate is

$$\dot{\lambda} = -\frac{\dot{v}_x}{\omega r_w} + \frac{v_x}{(\omega r_w)^2}\dot{\omega}r_w = -\frac{\mu(\lambda)F_z}{m_w\omega r_w} + \frac{1-\lambda}{\omega r_w}\dot{\omega}r_w \tag{44}$$

when the slip rate converges to the equilibrium point, $\dot{\lambda} = 0$,

$$\dot{\omega}r = \frac{\mu(\lambda)F_z}{m_w(1-\lambda)} = \frac{F_z}{m_w}\frac{\mu(\lambda)}{(1-\lambda)} \tag{45}$$

where, $\mu(\lambda)$ can be expressed by the modified Burckhardt tire model:

$$\mu(\lambda) = C_1 - C_1\exp[-\frac{C_2}{C_1}(\lambda + C_5\lambda^2)] - C_3\lambda sgn(\lambda) + C_4\lambda^2 \tag{46}$$

where, $C_i (i = 1, 2, 3, 4)$ are tire model factors that can be fitted according to tire test results.

From (45), the one-to-one correspondence between the angular acceleration and the slip rate can be obtained, when the slip rate is in a steady state.

Assuming that $F_z/m_w g$, we define the Angular Acceleration Coefficient (AAC)

$$\eta := \frac{\dot{\omega}r_w}{g} \tag{47}$$

and the AAC at the steady state slip rate is

$$\bar{\eta} = \frac{\mu(\lambda)}{1-\lambda} \tag{48}$$

Design the joint control variable

$$\varepsilon = \alpha\lambda + (1-\alpha)\eta, \quad 0 < \alpha < 1 \tag{49}$$

Figure 5 shows the $\mu - \lambda$ curve described by (46) and the reference slip rates on different road surfaces.

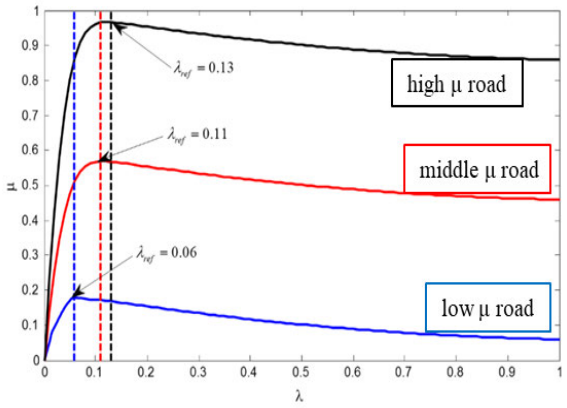

FIGURE 5. μ-λ curve and reference slip rates under different road adhesion conditions.

The $\bar{\eta} - \lambda$ curves are made based on the same tire model shown in Figure 5 and (48) shown in Figure 6. Corresponding to $\lambda = \lambda_{ref}$, $\bar{\eta} = \bar{\eta}_{ref}$ is marked with a horizontal line.

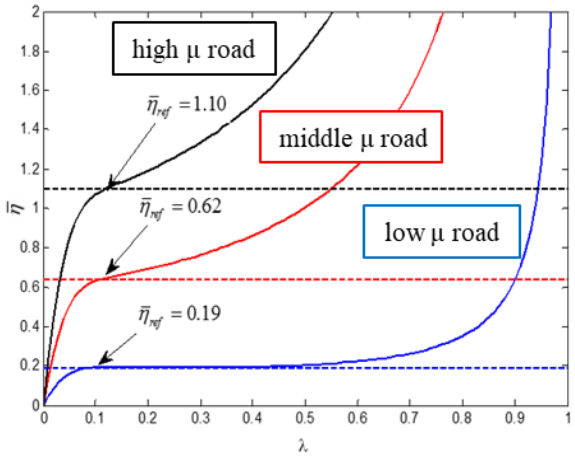

FIGURE 6. $\bar{\eta} - \lambda$ curves under different road adhesion conditions.

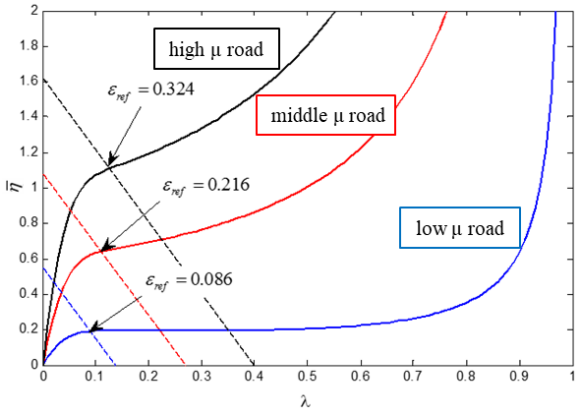

FIGURE 7. $\bar{\eta} - \lambda$ curve and joint controlled variables under different road adhesion conditions.

The reference joint control variable is described in (50) and Figure7.

$$\varepsilon_{ref} = \alpha\lambda_{ref} + (1 - \alpha)\bar{\eta}_{ref} \tag{50}$$

IV. SIMULATION AND EXPERIMENT

The simulation and experiment platform in this paper is a distributed drive electric vehicle with four in-wheel motors. The parameters of the vehicle and motor are shown in Table 1.

TABLE 1. Main parameters of the test vehicle.

Parameter	Value
Mass (kg)	1343.8
Wheel base (m)	2.305
Wheel track (m)	1.356
Height of COG (m)	0.54
Tire rolling radius (m)	0.29
Distance between COG and rear axle (m)	1.193
Motor peak torque (Nm)	320

A. LOW-FRICTION ROAD SIMULATION

The simulation was performed in the CarSim® and MATLAB/Simulink environment. In CarSim®, an initial vehicle speed of 0.1 km/h was set, the driver accelerated at full throttle, and the road adhesion coefficient was 0.2. To simulate the measurement of the signal noise and delay, white noise was added to the wheel speeds and longitudinal acceleration signals in Simulink, and we increased the time constant of the motor torque signal by a delay of 0.004 s. The simulation results are shown in Figure 8, where "w/o. ctrl." indicates the simulation without the proposed control method, and "w. ctrl." indicates the simulation with the control.

In the simulation, with the torque control of the ASR, the speed error finally converged to less than 2%, as shown in Figure 8(a). The joint control variable, which is composed of the slip rate and angular acceleration coefficient was used as the joint control variable of the controller, and $\alpha = 0.2$. Although the slip rate was not the only control variable, Figure 8(b) shows that the slip rate controlled by the ASR finally converged to the optimal slip rate of approximately 0.005; at the same time, Figure 8(c) shows that the final wheel angular acceleration also converged to $\bar{\eta}_{ref}$, which corresponds to the "low-adhesion road" shown in Figure 6. In Figures 8 (b) and (C), the wheel without ASR control seriously slipped; the slip rate and AAC decreased after a period of acceleration since the external characteristics of the motor at high speeds were limited and reduced the driving torque. Figure 8(d) shows the wheel torque received from the motor control unit when the vehicle was controlled by the proposed ASR. It has been proven that the joint control variable can ensure a good slip rate control effect when there are signal noise and estimation errors.

Table 2 shows a comparison of road adhesion utilization rates [calculated by (51)] when different α values and ±5% speed error were introduced.

$$\eta_{use} = \frac{\sum_{n=0}^{N}\sum_{i=1}^{4} F_{x,i}(n)}{\sum_{n=0}^{N}\sum_{i=1}^{4} \mu_i(n) F_{z,i}(n)} \tag{51}$$

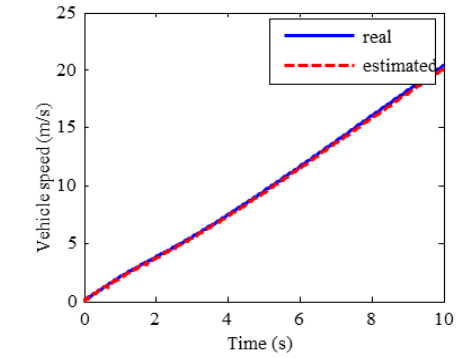

(a) Longitudinal speed (with control)

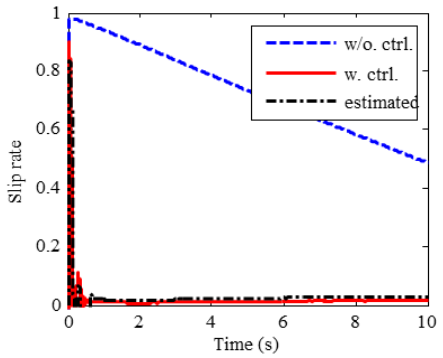

(b) Slip rate

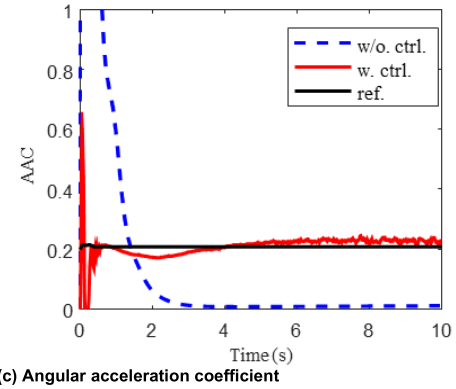

(c) Angular acceleration coefficient

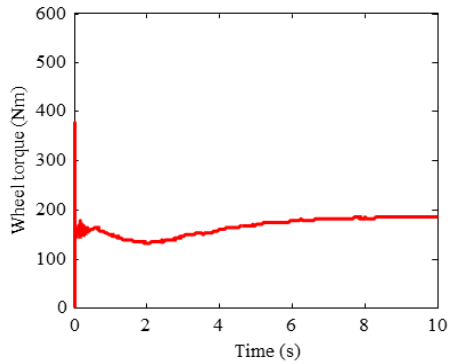

(d) Wheel torque (with control)

FIGURE 8. Simulation results on a low-friction road.

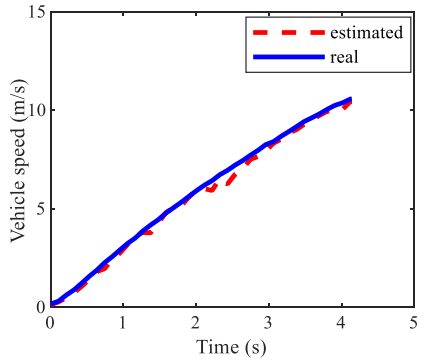

(a) Vehicle speed

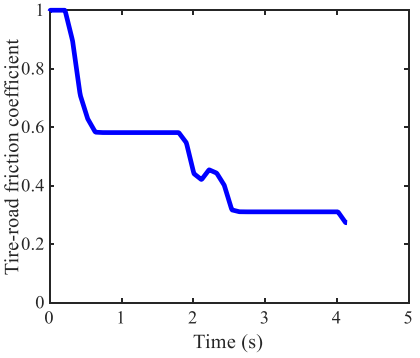

(b) Tire-road friction coefficient

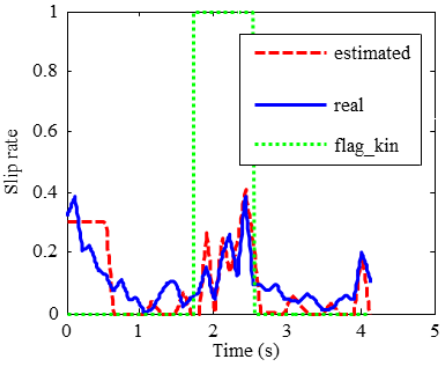

(c) Slip rate of the front left wheel

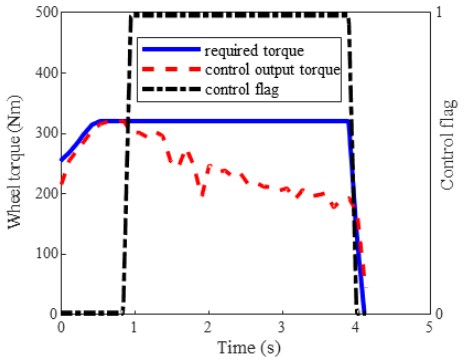

(d) Wheel torque of the front left wheel

FIGURE 9. Experiment results on a joint-friction road.

where, N is the number of operations in the simulation process.

Table 2 shows that under real vehicle speeds, compared to the slip rate control variable alone, the road adhesion utilization rate decreased by no more than 1% after using the joint control variable. In the case of vehicle speed estimation error, the results of the experimental group, which only used the slip rate as the control variable, significantly deteriorated;

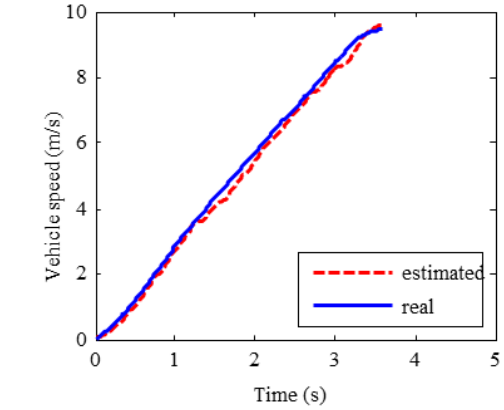

(a) Vehicle speed

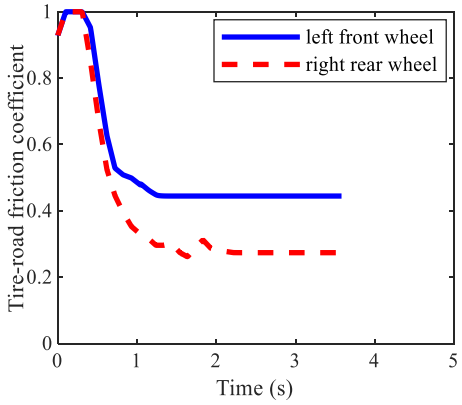

(b) Tire-road friction coefficient

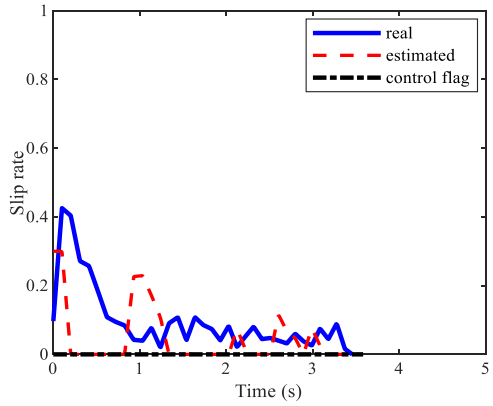

(c) Slip rate of the front left wheel

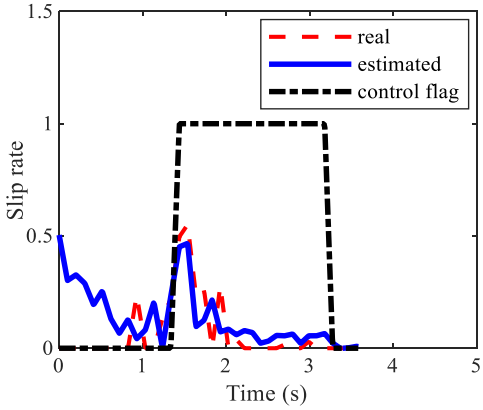

(d) Slip rate of the rear right wheel

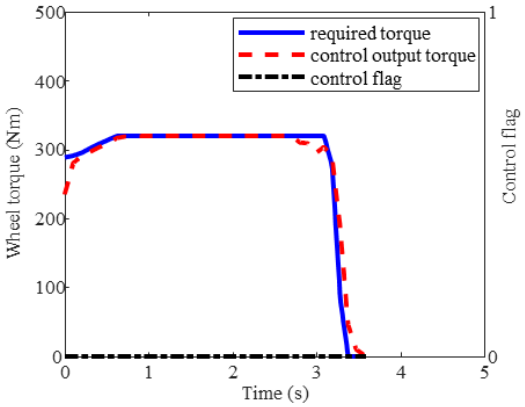

(e) Wheel torque of the front left wheel

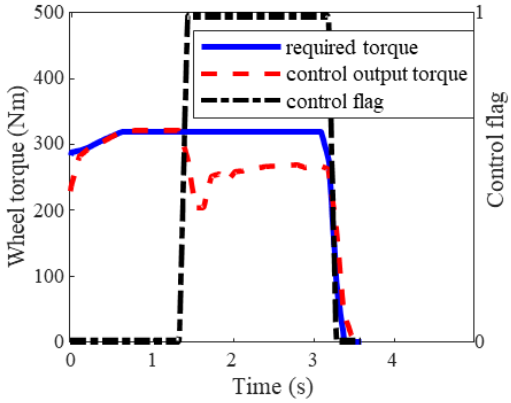

(f) Wheel torque of the rear right wheel

FIGURE 10. Experiment results on a split-friction road.

however, use of the joint control variable can maintain a high utilization rate of road adhesion and be robust against speed estimation errors.

B. JOINT-FRICTION ROAD EXPERIMENT

The test conditions were set as follows: the vehicle started on a dry tiled road and subsequently entered a wet tiled road. The test results are shown in Figure 9.

In Figure 9 (the same below), the "real" slip rate was calculated by (1), where the "real" vehicle speed was measured using a high-precision GPS and inertial navigation system (Oxford® RT 3003); the wheel speed, which was

TABLE 2. Comparison of the road adhesion utilization rates.

Condition	α=0.2	α=0.4	α=0.6	α=1.0 (only slip rate)
Real speed (Vr)	98.54%	99.05%	99.15%	99.42%
95% Vr	98.30%	96.67%	95.18%	92.06%
105% Vr	97.84%	95.21%	95.25%	95.24%
Estimated speed	97.51%	92.85%	91.52%	93.74%

equal to the in-wheel motor speed, was fed back from the motor control unit.

The tire-road peak adhesion coefficient estimated with the method proposed in [29] is shown in Figure 9(b). Figures 9(b) and (c) indicate that after the wheel entered the wet tile road and began to slip, the kinematic speed estimation method was activated ($flag\_kin = 1$) and switched to the dynamic estimator after a certain amount of time ($flag\_kin = 0$ when the dynamic and kinematic estimators worked alternately). The speed shown in Figure 9(a) indicates that after the vehicle entered the wet tile road, the speed estimation error gradually decreased with the intervention of the slip rate controller and dynamic speed estimator.

Figures 9(c) and (d) show that the slip rate control was not involved and that the motor provided the torque required by the driver when the vehicle was on the dry tile road. After the vehicle entered the low-adhesion road, the slip rate controller intervened to reduce the slip rate to the reference value, which effectively suppressed wheel skidding and ensured the driving performance of the vehicle. The proposed controller was robust against speed estimation errors and changes in the tire-road friction condition.

C. SPLIT-FRICTION ROAD EXPERIMENT

The experiment conditions were set as follows: the left wheel was on the dry tile road and the right wheel was on the wet tile road. The experiment results of the front left wheel and rear right wheel are shown in Figure 10.

Figure 10 shows that the wheel on the dry tile road did not excessively slide, and the slip rate control flag was 0; the controller of the wheel on the wet tile road was involved, and the slip rate gradually decreased to near the reference value to ensure stability.

V. CONCLUSION

In this paper, the robust variable structure slip rate control system for distributed drive electric vehicles is designed, including tire slip rate estimators, the speed estimator and the slip rate controller, that can calculate the slip rate in real time and make the joint control variable track its reference value using fast, precise and independent motor torque control.

1) Using the interaction between kinematic and dynamic estimation models, the dynamic model is adopted when the slip rate is small, which avoids the problem of the cumulative errors and the high dependence on the information quality of the sensors. In the case of a large slip rate, the kinematic method is adopted to estimate the vehicle speed, which avoids the problem of a decrease in tire model accuracy.

2) Based on the speed and slip rates obtained from low-cost sensors and the designed estimators, the joint control variable, which consists of the slip rate and angular acceleration coefficient, is proposed. The anti-windup sliding mode variable structure control law is designed, which shows good performance even in the presence of speed estimation error, and the asymptotic stability of the tracking error is proven by Lyapunov theory.

3) The results under various simulation and experimental conditions verify that the speed estimation algorithms can estimate the speed on both high- and low-adhesion roads well. The adopted slip rate control algorithm can intervene in time when the wheel is over skidding, restrain the rapid increase of the wheel slip rate, prevent serious wheel skidding on low-adhesion roads, ensure wheel stability and improve the vehicle driving performance.

REFERENCES

[1] L. Zhang, S. Zhang, and W. Zhang, "Multi-objective optimization design of in-wheel motors drive electric vehicle suspensions for improving handling stability," *Proc. Inst. Mech. Eng., D, J. Automobile Eng.*, vol. 233, no. 8, pp. 2232–2245, Jul. 2019.

[2] A. Zirek, P. Voltr, and M. Lata, "Validation of an anti-slip control method based on the angular acceleration of a wheel on a roller rig," *Proc. Inst. Mech. Eng., F, J. Rail Rapid Transit*, vol. 234, no. 9, pp. 1029–1040, Oct. 2020.

[3] L. Guo, H. Xu, and J. Zou, "Acceleration slip regulation control strategy for four-wheel independent drive electric vehicles," *IEEJ Trans. Electr. Electron. Eng.*, vol. 14, no. 4, pp. 630–639, Apr. 2019.

[4] S. Germann, M. Wurtenberger, and A. Daiss, "Monitoring of the friction coefficient between tyre and road surface," in *Proc. IEEE Int. Conf. Control Appl. (CCA)*, Glasgow, U.K., Aug. 1994, pp. 613–618.

[5] L. Chen, Y. Luo, M. Bian, Z. Qin, J. Luo, and K. Li, "Estimation of tire-road friction coefficient based on frequency domain data fusion," *Mech. Syst. Signal Process.*, vol. 85, pp. 177–192, Feb. 2017.

[6] Z. Zhang, B. Luan, X. Liu, and M. Zhang, "Effects of surface texture on tire-pavement noise and skid resistance in long freeway tunnels: From field investigation to technical practice," *Appl. Acoust.*, vol. 160, Mar. 2020, Art. no. 107120.

[7] S. Cheng, M.-M. Mei, X. Ran, L. Li, and L. Zhao, "Adaptive unified monitoring system design for tire-road information," *J. Dyn. Syst., Meas., Control*, vol. 141, no. 7, Jul. 2019, Art. no. 071006.

[8] L. Shao, C. Jin, C. Lex, and A. Eichberger, "Robust road friction estimation during vehicle steering," *Vehicle Syst. Dyn.*, vol. 57, no. 4, pp. 493–519, Apr. 2019.

[9] U. Kiencke and L. Nielsen, *Automotive Control Systems: For Engine, Driveline, and Vehicle*. Berlin, Germany: Springer, 2005.

[10] Y. Zhang, B. Leng, L. Xiong, Z. Yu, and D. Zeng, "Distributed drive electric vehicle longitudinal velocity estimation with adaptive Kalman filter: Theory and experiment," SAE Tech. Paper 2019-01-0439, 2019, doi: 10.4271/2019-01-0439.

[11] Y. Huang, L. Qian, A. Feng, Y. Wu, and W. Zhu, "RFID data-driven vehicle speed prediction via adaptive extended Kalman filter," *Sensors*, vol. 18, no. 9, p. 2787, Aug. 2018.

[12] H. Heidfeld, M. Schunemann, and R. Kasper, "Experimental validation of a GPS-aided model-based UKF vehicle state estimator," in *Proc. IEEE Int. Conf. Mechatronics (ICM)*, Ilmenau, Germany, Mar. 2019, pp. 537–543.

[13] C. E. Tannoury, F. Plestan, S. Moussaoui, and N. Romani, "Tyre effective radius and vehicle velocity estimation: A variable structure observer solution," in *Proc. 8th Int. Multi-Conf. Syst., Signals Devices*, Sousse, Tunisia, Mar. 2011, pp. 1–6.

[14] L. Imsland, T. A. Johansen, T. I. Fossen, J. C. Kalkkuhl, and A. Suissa, "Vehicle velocity estimation using modular nonlinear observers," in *Proc. 44th IEEE Conf. Decis. Control*, Seville, Spain, Dec. 2005, pp. 6728–6733.

[15] Z.-G. Zhao, L.-J. Zhou, J.-T. Zhang, Q. Zhu, and J.-K. Hedrick, "Distributed and self-adaptive vehicle speed estimation in the composite braking case for four-wheel drive hybrid electric car," *Vehicle Syst. Dyn.*, vol. 55, no. 5, pp. 750–773, May 2017.

[16] F. Liu, J. Zhou, J. Chen, and X. Yin, "An approach of trajectory estimation for high-speed unmanned skid-steered vehicle," in *Proc. Int. Conf. Energy, Ecol. Environ. Int. Conf. Electr. Intell. Vehicles*, Melbourne, VIC, Australia, Nov. 2018, pp. 1–6.

[17] F. Li and Z. Liu, "Study on control logic and simulation of 4 wheel drive vehicle ASR," in *Proc. 3rd Int. Conf. Mech. Syst. Mater. Appl.*, Singapore, May 2017, pp. 46–52.

[18] D. Savitski, D. Schleinin, V. Ivanov, K. Augsburg, E. Jimenez, R. He, C. Sandu, and P. Barber, "Improvement of traction performance and off-road mobility for a vehicle with four individual electric motors: Driving over icy road," *J. Terramechanics*, vol. 69, pp. 33–43, Feb. 2017.

[19] S. De Pinto, C. Chatzikomis, A. Sorniotti, and G. Mantriota, "Comparison of traction controllers for electric vehicles with on-board drivetrains," *IEEE Trans. Veh. Technol.*, vol. 66, no. 8, pp. 6715–6727, Aug. 2017.
[20] D. Tavernini, M. Metzler, P. Gruber, and A. Sorniotti, "Explicit nonlinear model predictive control for electric vehicle traction control," *IEEE Trans. Control Syst. Technol.*, vol. 27, no. 4, pp. 1438–1451, Jul. 2019.
[21] K. Hartani, M. Khalfaoui, A. Merah, and N. Aouadj, "A robust wheel slip control design with radius dynamics observer for EV," *SAE Int. J. Vehicle Dyn., Stability, NVH*, vol. 2, no. 2, pp. 135–146, Jun. 2018.
[22] P. Wang, S. Gao, L. Li, S. Cheng, and L. Zhao, "Automatic steering control strategy for unmanned vehicles based on robust backstepping sliding mode control theory," *IEEE Access*, vol. 7, pp. 64984–64992, 2019.
[23] V. Gowda and A. Ramachanrda, "Modelling and performance evaluation of anti-lock braking system," *J. Eng. Sci. Technol.*, vol. 14, no. 5, pp. 3028–3045, Oct. 2019.
[24] J.-C. Wang, R. He, and Y.-B. Kim, "Optimal control of regenerative hydraulic composite braking system based on a voltage variable charging control scheme," *Proc. Inst. Mech. Eng., D, J. Automobile Eng.*, vol. 234, nos. 2–3, pp. 536–551, Feb. 2020.
[25] Z. Huang, W. Du, B. Chen, K. Gao, Y. Liu, X. Tang, and Y. Yang, "An online super-twisting sliding mode anti-slip control strategy," *Energies*, vol. 13, no. 7, p. 1823, Apr. 2020.
[26] D. Savitski, V. Ivanov, K. Augsburg, T. Emmei, H. Fuse, H. Fujimoto, and L. M. Fridman, "Wheel slip control for the electric vehicle with in-wheel motors: Variable structure and sliding mode methods," *IEEE Trans. Ind. Electron.*, vol. 67, no. 10, pp. 8535–8544, Oct. 2020.
[27] L. Zhang, Y. Wang, and Z. Wang, "Robust lateral motion control for in-wheel-motor-drive electric vehicles with network induced delays," *IEEE Trans. Veh. Technol.*, vol. 68, no. 11, pp. 10585–10593, Nov. 2019.
[28] R. de Castro, R. E. Araujo, and D. Freitas, "Wheel slip control of EVs based on sliding mode technique with conditional integrators," *IEEE Trans. Ind. Electron.*, vol. 60, no. 8, pp. 3256–3271, Aug. 2013.
[29] X. Xia, L. Xiong, K. Sun, and Z. P. Yu, "Estimation of maximum road friction coefficient based on Lyapunov method," *Int. J. Automot. Technol.*, vol. 17, no. 6, pp. 991–1002, Dec. 2016.

BO LENG received the B.S. and Ph.D. degrees in vehicle engineering from the School of Automotive Studies, Tongji University, Shanghai, China, in 2014 and 2019, respectively. He is currently working as a Postdoctoral Researcher with the Postdoctoral Station of Mechanical Engineering and the School of Automotive Studies, Tongji University. His research interests include vehicle dynamics and control, distributed drive electric vehicle, motion control, state and parameter estimation, and intelligent vehicle trajectory planning.

LU XIONG received the M.S. and Ph.D. degrees in vehicle engineering from Tongji University, Shanghai, China, in 2002 and 2005, respectively.

He is currently a Professor and a Doctoral Supervisor with the School of Automotive Studies, Tongji University. He also works as the Associate Director of the Clean Energy Automotive Engineering Center, Tongji University, which is the National Engineering Laboratory for New Energy Vehicle and Powertrain of China. His research interests include electric vehicle, intelligent vehicle, and all-terrain vehicle. He has won the first prize of the Shanghai Science and Technology Progress Awards, in 2013 and 2019, respectively.

ZHUOPING YU received the M.S. degree from Tongji University, Shanghai, China, in 1985, and the Ph.D. degree from Tsinghua University, Beijing, China, in 1996.

He is currently a Professor and a Doctoral Supervisor with the School of Automotive Studies, Tongji University. He is also the Director of the National Collaborative Innovation Center for Intelligent New Energy Vehicle of China, and a Fellow and Vice Chairman of the China Automotive Engineering Society. His research interests include electric vehicle, fuel cell vehicle, and intelligent vehicle. He has won the Second Prize of the China Science and Technology Progress Award in 2008, the first prize of the Shanghai Science and Technology Progress Awards in 2013 and 2019, and the Grand Prize of the Science and Technology Progress in Automotive Industry in 2019.

KAI SUN received the B.S. degree in vehicle engineering from the School of Mechanical Engineering, Beijing Institute of Technology, Beijing, in 2014, and the M.S. degree in vehicle engineering from the School of Automotive Studies, Tongji University, Shanghai, in 2017. His research interests include slip rate control, parameter estimation, and advanced driver assistance systems.

MING LIU received the B.S. degree in vehicle engineering from the College of Mechanical and Vehicle Engineering, Hunan University, Changsha, Hunan, in 2019. He is currently pursuing the M.S. degree in vehicle engineering with the School of Automotive Studies, Tongji University, Shanghai. His research interests include slip rate control and trajectory tracking.